Using Penman-Monteith Method to Estimate Potential Evapotranspiration in Taiwan by Using AVHRR and MODIS Satellites Remote Sensing Data

Chen Min, Kuo
Department of Hydraulic and Ocean Engineering, National Cheng Kung University
1 Ta-Hsueh Rd., Tainan, Taiwan.
n8890102@ccmail.ncku.edu.tw

Pao Shan, Yu
Department of Hydraulic and Ocean Engineering, National Cheng Kung University
1 Ta-Hsueh Rd., Tainan, Taiwan.
yups@mail.ncku.edu.tw

Rong Hong, Du
Department of Hydraulic and Ocean Engineering, National Cheng Kung University
1 Ta-Hsueh Rd., Tainan, Taiwan.
n8692110@ccmail.ncku.edu.tw

Chin Yuan, Lin
Department of Hydraulic and Ocean Engineering, National Cheng Kung University
1 Ta-Hsueh Rd., Tainan, Taiwan.
n8693419@ccmail.ncku.edu.tw

Abstract: Recent advances in remote sensing technology have led to ways of estimating regional evapotranspiration from AVHRR satellite images. The newly developed MODIS satellite is being increasingly used in estimating evapotranspiration. This study aims to estimate the meteorological characteristics of Penman-Monteith method from AVHRR and MODIS images and then the evapotranspiration results are compared. Four major meteorological characteristics (air temperature, vapor pressure deficit, wind speed, and net radiation) were derived from images and station observations. The average errors of the evapotranspiration estimation were 1.197 mm/day (AVHRR) and 0.63 mm/day (MODIS), and the relative root-mean-squared errors were 0.477 (AVHRR) and 0.288 (MODIS). The verification results revealed that both MODIS and AVHRR images can be applied to estimate evapotranspiration, in which the estimation using MODIS images is better. Amount these four meteorological characteristics, the net radiation has the best estimation and the win speed was the poorest. However, the most sensitivity of the net radiation has led the worst result in estimating evapotranspiration. The accurately estimation of the net radiation is necessary in the future. Totally, the influence by the error of each meteorological characteristic was less than 11%. This suggested that this method with MODIS images is useful and practical in regional potential evapotranspiration estimation and can be suitably used in ungauged areas.
Keywords: Regional Potential Evapotranspiration, Satellite Remote Sensing, AVHRR, MODIS.

1. Introduction

Evapotranspiration is a key component of water resource management influencing the water demands of agriculture and domesticity. The stationary observations previously used to compute evapotranspiration cannot yield the amounts of large areas. Since the ungauge area was difficult to measure, remote sensing has been employed to develop practical evapotranspiration estimation methods. Remote sensing allows engineers to obtain regional land surface information easily, and decreases the required manpower in field observations.

Recently, the evapotranspiration was derived from Landsat satellite and NOAA-AVHRR (National Oceanic and Atmospheric Administration of the United States, Advanced Very High Resolution Radiometer) satellite images. The evapotranspiration was estimated from Landsat series satellite images using energy balance method (Seguin and Iterier, 1983[17]; Menenti and Choudhury, 1993[13]; Laymon, 1998[12]; Farah and Bastiaanssen, 2001[6]). The energy fluxes (soil heat flux, sensible heat flux, and latent heat flux) of the energy balance method were derived from images except the net radiation which was from the observation. Therefore, they cannot represent the variation from different land uses. In NOAA-AVHRR satellites (Bella, 2000[2]; Boni *et al.*, 2001[4]; Jiang and Islan, 2001[11]), the image-derived surface temperature was in establishing the regression equation with evapotranspiration. However, this scheme cannot represent the regional variation of evapotranspiration either. Granger (1997[7], 2000[8]) demonstrated a novel scheme applying

remote sensing data in estimating evapotranspiration with Penman method. The required variables of Penman method were derived from the AVHRR satellite images by regression analysis. By this method, the remote sensing application could estimate the regional evapotranspiration, without using the atmospheric data observed at ground level. Unfortunately, the regression parameters and the Penman method were not suitable for use in Taiwan.

Since the newly development of MODIS (Moderate Resolution Imaging Spectroradiometer) images, it served more channels and higher resolution than AVHRR. As the applications of MODIS images were more convenient. Czajkowski *et al.* (2002)[5] suggested that Channel 31 and 32 of MODIS can include the same information as Channel 4 and 5 of AVHRR, and can be employed to derive the temperature. Channel 29 of MODIS can be employed to detect the water vapor. Venturini *et al*. (2004)[19] applied the temperature and NDVI (Normalization difference vegetation index) which were derived from AVHRR and MODIS to estimate the evaporative fraction in south Florida to estimate the latent heat flux of the energy budget. Then, the latent heat was transferred to represent the evapotranspiration. However, few applications of MODIS have been used in estimating evapotranspiration.

From the researches above, both the AVHRR and MODIS images can use for estimating evapotranspiration. However, these methods are not convenient for engineers. They need a simpler method to estimate evapotranspiration from images directly. This study aimed to follow the Granger (1997[7], 2000[8]) theory to derive the meteorological characteristics of Penman-Monteith method to estimate regional potential evapotranspiration in Taiwan. Both the AVHRR and MODIS images were used, and compared with the observation data to determine which image obtained the most appropriate result.

2. Study area and methodology

1) Study area

This study aimed to establish an appropriate regional evapotranspiration scheme. The immobile methodology was required for all Taiwan, not just locally. AVHRR and MODIS images have been chosen to cover the whole of Taiwan, and applied to establish the regional meteorological characteristics. The topography of Taiwan is divided into the western plain, and the eastern mountainous region. Western Taiwan is densely populated and has heavy water resource requirements. Therefore, this study focuses on western Taiwan, which contains 13 main meteorological stations. These stations were selected as the reference ground truth to determine the appropriate evapotranspiration estimation scheme. Fig. 1 lists the main meteorological stations and the topography they cover.

2) Methodology for estimating evapotranspiration

Most evapotranspiration methods are based on energy balance method. Since Penman (1948)[15] successfully combined the aerodynamic approaches and energy balance to estimate evapotranspiration, most methods also define the vapour transfer using the vapour pressure and wind function. Monteith (1965)[14] replaced the wind function with the crop canopy and aerodynamic resistance to decrease the regional variation forming the Penman-Monteith method. The FAO (Food and Agricultural Organization) Penman-Monteith method for calculating potential evapotranspiration can be expressed as (Allen *et al.*, 1998[1]):

$$ET_0 = \frac{0.408\Delta(R_n - G) + \gamma \frac{900}{(T+273)} u(e_s - e_a)}{\Delta + \gamma(1 + 0.34u)} \quad (1)$$

where

ET_0 =daily reference crop evapotranspiration (mm day^{-1}),

R_n =net radiation flux density (MJ m^{-2} day^{-1}),

G =heat flux density into the soil (MJ m^{-2} day^{-1}), it is very small and can be neglected,

T =mean daily air temperature (^oC),

γ =psychrometric constant (kPa $^oC^{-1}$),

u =wind speed measured at 2m height (m s^{-1}),

e_s =saturation vapor pressure (kPa), $e_s = 0.611 exp\left(\frac{17.27T}{T+237.3}\right)$

e_a =actual vapor pressure (kPa), $e_a = e_s \times \frac{RH}{100}$

RH : relative humidity (%),

e_s–e_a =saturation vapour pressure deficit (kPa),

Δ =slope of saturation vapour pressure curve (kPa °C^{-1}), $\Delta = \frac{4098e_a}{(T+237.3)^2} = \frac{2504exp\left(\frac{17.27T}{T+237.3}\right)}{(T+237.3)^2}$

The Penman-Monteith method's characteristics listed above, can be integrated into four major meteorological characteristics - mean daily air temperature (T), saturation vapor pressure deficit (e_s–e_a), wind speed (u) and net radiation flux density (R_n).

This study aimed to estimate the regional evapotranspiration except using stationary observation. We tried to establish the relationships to estimate the four major meteorological characteristics from satellite images and meteorological observation.

3. Data acquired from AVHRR and MODIS images

NOAA has launched a series of weather satellites with a processing project. NOAA satellites have some scientific sensors. One sensor, AVHRR, was employed to determine the cloud coefficients and sea surface temperature. The AVHRR sensor includes five channels, one visible channel (ch1), one near infrared channel (ch2) and three thermal infrared channels (ch3,4,5). The thermal infrared (TIR) channels are employed to calculate the sea surface temperature. The temperature appears to be significant distinguishing in TIR channels. Hence, the TIR channels, ch4 and ch5, of AVHRR were applied to estimate the land surface temperature.

The MODIS instruments were aboard on Terra and Aqua satellites, which were lunched in 1999 (Terra) and 2002 (Aqua). The Terra satellite passes over Taiwan at 10:30, and the Aqua satellite passes over Taiwan at 13:30. The Terra and Aqua MODIS acquire data with 36 spectral bands and the resolutions of MODIS were 250m (ch1–2), 500m (ch3–7) and 1000m (ch8–36). Channels 1, 2, 31 and 32 of MODIS, which are equivalent to those in AVHRR, were selected to obtain the meteorological characteristics. The similar wave-length of AVHRR and MODIS were described in Table.1.

Most evapotranspiration arose during the daytime. Among the NOAA series satellites, NOAA-14 passes Taiwan at 1400-1600 every day. We chose NOAA-14 AVHRR images and MODIS (Terra and Aqua) images that are appropriate for estimating evapotranspiration. We collected 59 AVHRR images and 12 MODIS images during 1999 and 2004.

To prevent seasonal influence, all images were acquired at various times from January through December. After geometrical correction, the digital number (DN) of the main meteorological stations can be accurately acquired from images. Then, the channel radiance (I_λ, λ means the channel) and brightness temperature (T_λ, λ means the channel) was derived from the DN.

4. Potential evapotranspiration estimation

1) Meteorological characteristics

After cloud filtering, 466 AVHRR pixels and 246 MODIS pixels remained. All remaining pixels included efficient information and were employed to derive meteorological characteristics. As mentioned in Section 2.2, the meteorological characteristics of Penman-Monteith method, mean daily air temperature (T), saturation vapor pressure deficit (e_s-e_a), wind speed (u) and net radiation flux density (R_n), were used to estimate the regional evapotranspiration. Satellite images are helpful to obtain the regional estimation in the ungauge area. These meteorological characteristics were tried to establish the relationship with AVHRR images and MODIS images. The available image pixels were randomly split into simulated and verified sets to determine the accuracy of this method. The simulated set contained 160 AVHRR pixels and 184 MODIS pixels for simulation, and the remaining pixels were used in validation.

Mean daily air temperature

Temperature is a key factor in the Penman-Monteith method, since it reflected the amount of solar energy. Granger (2000) and Prata and Platt (1991)[16] introduced a split-window technique to estimate temperature, and demonstrated good agreement with the observation data. Nevertheless, these methods employed both the brightness temperature and surface emissivities, and they did not show good agreement in the study area herein. Therefore, we tried to derive a new relationship function and simplified the parameters by only using the brightness temperature.

Channels 4 and 5 of AVHRR were usually used for estimating the temperature. The brightness temperature, T_4 and T_5, were employed to identify the relationship with mean daily air temperature. The relationship for mean daily air temperature is given as:

$$T = 9.633 + 3.387T_4 - 3.103T_5 \quad (2)$$

The simulated and verified results were shown in Fig. 2, where the T_{sim} is the simulated mean daily air temperature derived from Eq.(2) and T_{obs} is the mean air temperature observed from meteorological stations. The simulated mean daily air temperature derived from Eq.(2) demonstrated good agreement with the observation. The accuracy of this relationship, R^2, from simulated set was 0.717, and the R^2 of verified set was 0.722. It reveals that the surface temperature can be represented using T_4 and T_5 of AVHRR images.

The channels 31 and 32 of MODIS can serve the same data as AVHRR channels 4 and 5. We followed the method used in AVHRR temperature derivation. However, the brightness temperature of channels 31 and 32 could not represent the actual air temperature well. For the reason to use the limited information from images only, we have tested the radiance and NDVI. It was found that the brightness temperature (T_{31}, T_{32}) and NDVI were applicable established the relationship function with the mean daily air temperature (T). The relationship is given as:

$$T = 3.566 + 4.092T_{31} - 3.464T_{32} - 6.089NDVI \quad (3)$$

As shown in Fig. 3, the simulated R^2 was 0.84, and the validated R^2 was 0.76. The analytical results exhibited that the MODIS images have good agreement with the mean air temperature observed from meteorological stations.

Saturation vapor pressure deficit

Granger (2000)[8] successfully applied the long-term mean air temperature and saturated vapor pressure to obtain the regression function of saturation vapor pressure deficit. Actually, the saturated vapor pressure bases on a nonlinear function of temperature. Therefore, the saturation vapor pressure deficit can be simplified to determine from the saturated vapor pressure. And we calculated the saturated vapor pressure by using the mean daily average air temperature from Eq.(2) and Eq.(3), instead of the long-term mean air temperature applied by Granger (2000)[8].

The relationship of saturation vapor pressure deficit derived from AVHRR is shown below.

$$VP_{def} = 0.23e_a + 0.5573 \quad (4)$$

where, VP_{def} = saturation vapor pressure deficit, $VP_{def} = e_s - e_a$

The simulated and verified results were shown in Fig. 4, where $VP_{def\ sim}$ means the saturation vapor pressure deficit from Eq.(4) and the $VP_{def\ obs}$ means the saturation vapor pressure deficit calculate from RH and e_s observation. The simulated R^2 was 0.554, and the validated R^2 was 0.516. The relationship was acceptable for further application.

In the derivation from MODIS images, the saturated vapor pressure could not represent the saturation vapor pressure deficit well. For the same reason with the estimation in temperature, we tried to establish the relationship with other available data from images. We found that the saturated vapor pressure and reflectance of Channel 1(r_1) can exhibit the better agreement with vapor pressure deficit. The relationship function is presented below.

$$VP_{def} = 0.438e_a - 4.573r_1 + 0.5573 \quad (5)$$

The simulated and verified results were shown in Fig. 5. The simulated R^2 was 0.47, and the validated R^2 was 0.57.

Both the AVHRR and MODIS were not very good in estimating the saturation vapor pressure deficit. Because of the available of data from images was not enough. However, the regression results were accepted, and were considered in the following work.

Net radiation

The net radiation is computed as the difference between the net short-wave radiation and net long-wave radiation, as:

$$R_n = (1-\alpha)R_s + R_l^{\downarrow} - R_l^{\uparrow} \quad (6)$$

where

α=albedo

R_s= incoming short-wave radiation (MJ m^{-2} day^{-1})

$R_l^{\downarrow}$=incoming long-wave radiation (MJ m^{-2} day^{-1})

$R_l^{\uparrow}$=reflecting long-wave radiation (MJ m^{-2} day^{-1})

The incoming short-wave radiation was affected by the month and latitude. We adopt the mean solar radiation, which was list in Table 2(Jensen *et al.*, 1990[10]) to represent the incoming short-wave radiation.

After estimating the incoming short-wave radiation, the albedo and the sunshine duration are needed in Penman-Monteith method. The albedo, usually set as 0.23, was only used for the evergreen plant surface and is inappropriate for

the heterogeneous surface. Gutman (1988) [9] proposed substituting the radiance of AVHRR ch1 and ch2 (I_1, I_2) for the surface albedo. Granger (1997)[7] demonstrated that the albedo can be replaced by the radiance of AVHRR ch2 (I_2). With the similar wave-length range of MODIS ch2 and AVHRR ch2, the albedo from MODIS image was represented by the radiance of ch2.

In Penman-Monteith method, the duration of sunshine is used to determine the long-wave radiation. The duration of sunshine was defined as the period when the direct solar radiation exceeded 120 W/m^2. However, an instantaneous satellite image cannot be used to compute the duration of sunshine. Therefore, the calculations of long-wave radiation were followed the Stefan-Boltzmann law. (Prata and Platt, 1991[16])

$$R_l^{\downarrow} = e_{sky}\sigma T^4 \tag{7}$$

$$R_l^{\uparrow} = \sigma T_s^4 \tag{8}$$

where,

T =air temperature

T_s =surface temperature

e_{sky} =emissivity

Wind speed

The wind speed is measured on site. For the instantaneous satellite snapshot, the remote sensing data cannot describe the wind speed easily. Yu *et al.* (2002)[18] tested the sensitivity of meteorological characteristics in modified Penman equation, and suggested that the wind speed is the least sensitivity variable. We tested the sensitivity of wind speed in Penman-Monteith method. All stations' observations from 1950 to 2000 were acquired and the results were illustrated in Fig.6. Where, the net radiation (R_n) and the wind speed (u) were the largest and least sensitivity variables in the Penman-Monteith method. The evapotranspiration varies ±80% as the variation of net radiation is ±80%. And the evapotranspiration varies ±10% as the variation of wind speed is ± 80%. This result was similar to Beven (1979)[3], that the net radiation was the most sensitivity variable of Penman-Monteith method. Hence, this study took the long-term monthly average wind speed into the Penman-Monteith method.

2) Potential evapotranspiration verification

Two indexes, the relative Root-Mean-Square Error (RMSE) and the Mean Error (ME) are used to compare the potential evapotranspiration estimated from images (PET_{RS}) and the pen evapotranspiration (PanET) to verify the results.

$$RMSE = \sqrt{\frac{\sum_{t=1}^{n}\left[\left(AE_t - E_t\right)/AE_t\right]^2}{n}} \tag{9}$$

$$ME = \frac{\sum_{t=1}^{n}\left|AE_t - E_t\right|}{n} \tag{10}$$

Where, the AE_t means the PanET, E_t means the PET_{RS}, and n means the amount of calculation.

Because of lacking the observations (Tainan and Hsinchu stations) of PanET in two meteorological stations, only 397 (AVHRR) and 203 (MODIS) PET_{RS} results can be used to verify with PanET. The verification was listed in Table 3. Based on the average RMSE and ME values, the estimate from MODIS is much better than that from AVHRR. The comparison of PanET and PET_{RS} was shown in Fig.7. Both AVHRR and MODIS can well estimate the potential evapotranspiration with Penman-Monteith method, and the MODIS calculations agree better with the observed data than those from AVHRR.

5. Discussion

After introducing the method of estimating the potential evapotranspiration from AVHRR and MODIS images with Penman-Monteith method, it showed that the MODIS images have the better estimation than AVHRR images. Then we discussed the major error source in this method, and we focused on MODIS images in following discussion.

First, the accuracy of the Penman-Monteith method was tested. The meteorological characteristics from meteorological stations were applied to the Penman-Monteith method and leaded potential evapotranspiration ($PET_{PM\ Obs}$). It was compared with the PenET and the result was shown in Fig. 8. The mean error was 0.77 mm/day and the RMSE was 0.57.

From the comparison, the Penman-Monteith method has the overestimating problem. It was the original error of the Penman-Monteith method. Then, we compared the PET_{RS} from MODIS images and $PET_{PM\ Obs}$ as shown in Fig. 9. It showed good agreement and the errors were relatively small, the mean error was 0.63 mm/day and the RMSE decreased to 0.23. From the analysis above, we can conclude that there has some error in the Penman-Monteith method itself. So, the PET_{RS} from MODIS images was acceptable.

Then, we discussed the influences of meteorological characteristics. The error of each meteorological characteristic was discussed first. We compared the meteorological characteristics from observation and that in section 4.1. The average percentage of relative error (RE) of each meteorological characteristic was listed in Table 4.

Where, $$RE = \frac{\sum_{t=1}^{n}\left(\frac{\left|AE_t - E_t\right|}{AE_t}\times 100\%\right)}{n} \quad (11)$$

The wind speed (u) has the largest error (RE=52.9%), and the net radiation (R_n) was the least (RE=11.0%). It seems that error of estimation was come from wind speed. But, the sensitivity of each meteorological characteristic to Penman-Monteith method has to be considered. After the sensitivity correction, the influence of meteorological characteristics to Penman-Monteith method was listed in Table 4. Because of the least sensitivity with wind speed, the influence of wind speed decreased to 9.3%. The influence of net radiation is the largest (10.3%), although it was very close to stationary observation.

Then, we focused on the Penman-Monteith method and replaced each meteorological characteristic from observation to the ones we use in this method. For example of mean daily air temperature, we would estimate the potential evapotranspiration with Penman-Monteith method by using the observation data first, and compare with the result with using the mean daily air temperature that was estimated in section 4.1. Then, the comparison would show the influence by the mean daily air temperature. The mean error (ME) and the average percentage of relative error (RE) were listed in Table 5.

The influence by the net radiation (R_n) was the largest (ME=0.35 mm/day, RE=10.17%) and the mean daily air temperature (T) was the least (ME=0.25 mm/day, RE=6.69%). This result was similar to the one in Table 4.

We can summarize that the key factor of this study is the net radiation, and the mean daily air temperature has the least influence. We need more accurately estimation of the net radiation.

6. Conclusion

Evapotranspiration is a key factor in water resources estimation, influencing the water budget in a catchment. Station evapotranspiration does not reliably represent the regional evapotranspiration. Satellite remote sensing can provide the stipulated spatial heterogeneity of the catchments and help to understand the ungauge area. The development of potential evapotranspiration estimation from remote sensing is very helpful in water resource decision-making. This study compared two different satellites, AVHRR and MODIS, to obtain high-quality regional potential evapotranspiration estimation.

The meteorological characteristics of the Penman-Monteith method can generalize to four characteristics - temperature, vapor pressure deficit, wind speed and net radiation. Since the wind speed cannot be estimated from satellite, the relationships were proposed to derive the other meteorological characteristics from satellite images. The validations reveal that the mean errors of AVHRR and MODIS are 1.197 mm/day and 0.630 mm/day, and the root-mean-square error of AVHRR and MODIS are 0.477 and 0.288. The potential evapotranspiration estimation shows that both the AVHRR and MODIS images exhibit good agreement with observation data. However, the estimation from MODIS is better than that from AVHRR. Then, the accuracy of Penman-Monteith method and the influences of meteorological characteristics have been discussed. The Penman-Monteith method was overestimated with using stationary observation. Moreover, the influences of PET estimation is due to the error of each meteorological characteristic were less than 11% and the key factor is the net radiation. Therefore, this study concludes that we can estimate the potential evapotranspiration with Penman-Monteith method by using the meteorological characteristics with MODIS images.

7. Acknowledgment

The authors would like to thank Prof. Liu, Gin-Rong and Prof. Liu, Yuei-An for supporting NOAA-AVHRR and MODIS images. The authors would like to thank Dr. Lin, Tang-Haang for leading us image processing techniques. This study was supported by the National Science Council of the Republic of China, Taiwan for financially supporting this research (NSC-91-2211-E-006-038).

References

[1] Allen, R. G., L. S. Pereira, D. Raes, and M. Smith, 1998. Crop evapotranspiration- Guidelines for computing crop water requirements, FAO Irrigation and Drainage Paper 56, FAO, ISBN 92-5-104219-5.

[2] Bella, C. M. D., C. M. Rebella, and J. M. Paruelo, 2000. Evapotranspiration estimates using NOAA AVHRR imagery in the Pampa region of Argentina, *International Journal of the Remote Sensing*, 21(4): 791-797.

[3] Beven, K., 1979. A Sensitivity Analysis of the Penman-Monteith Actual Evapotranspiration estimates, *Journal of Hydrology*, 44:169-190.

[4] Boni, G., D. Entekhabi, and F. Castelli, 2001. Land data assimilation with satellite measurements for the estimation of surface energy balance components and surface control on evaporation, *Water Resource Research*, 37(6): 1713-1722.

[5] Czajkowski, K. P., S. N. Goward, D. Shirey, and A. Walz, 2002. Thermal remote sensing of near-surface water vapor, *Remote Sensing of Environment*, 79: 253-265.

[6] Farah, H. O., and W. G. M. Bastiaanssen, 2001. Impact of spatial variations of land surface parameters on regional evaporation: a case study with remote sensing data, *Hydrological Processes*, 15: 1585-1607.

[7] Granger R. J., 1997. Comparison of surface and satellite-derived estimates of evapotranspiration using a feedback algorithm. Application of remote sensing in hydrology, *Proceedings of the Third International Workshop*, NHRI Symposium, 17, pp.71-81.

[8] Granger, R. J., 2000. Satellite-derived estimates of evapotranspiration in the Gediz basin, *Journal of Hydrology*, 229: 70-76.

[9] Gutman, G., 1988. A simple method for estimating monthly mean albedo of land surface from AVHRR data, *Journal of Applied Meteorology*, 27: 973-988.

[10] Jensen, M. E., R. D. Burman, and R. G. Allen, 1990. Evapotranspiration and irrigation water requirement, American Society of Civil Engineers, New York.

[11] Jiang, L., and S. Islam, 2001. Estimation of surface evaporation map over southern Great Plains using remote sensing data, *Water Resources Research*, 37(2): 329-340.

[12] Laymon, C., D. Quattrochi, E. Malek, L. Hipps, J. Boettinger, and G. McCurdy, 1998. Remotely-sensed regional-scale evapotranspiration of a semi-arid Great Basin desert and its relationship to geomorphology, soils, and vegetation, *Geomorphology*, 21: 329-349.

[13] Menenti, M., and Choudhury, B. J., 1993, Parameterization of land surface evaporation by means of location dependent potential evaporation and surface temperature range. *Proceedings of IAHS conference on Land Surface Processes*, IAHS Publ., 212, pp.561-568.

[14] Monteith, J. L., 1965. Evaporation and environment, In: The state and movement of eater in living organism. G. E. Fogg (Ed.), Cambridge University Press, 205–234.

[15] Penman, H. L., 1948. Natural evaporation from open water, bare soil and grass, *Proc. R. Soc. London Ser*. A, 193, 120-145.

[16] Prata, A. J., and C. M. R. Platt, 1991. Land surface temperature measurements from the AVHRR, *Proceeding of The 5th AVHRR Data Users' Meeting*, Tromso, Norway, pp.433-438.

[17] Seguin, B., and B. Itier, 1983. Using midday surface temperature to estimate daily evaporation from satellite thermal IR data, *International Journal of Remote Sensing*, Vol. 4(2): 371-383.

[18] Yu, P.S., T. C. Yang, and C. C. Chou, 2002. Effect of climate change on evapotranspiration from paddy fields in southern Taiwan, *Climatic Change*, 54(1-2): 165-179.

[19] Venturini, V., G. Bisht, S. Islam, and L. Jiang, 2004. Comparison of evaporative fractions estimated from AVHRR and MODIS sensors over South Florida, *Remote Sensing of Environment*, 93: 77-86.

Table 1. The wave-length of AVHRR and MODIS

AVHRR			MODIS		
Channel	Range of wave length		Channel	Range of wave length	
1	0.58 - 0.68 μm	VIS	1	0.62 - 0.67 μm	VIS
2	0.725 - 1.1 μm	NIR	2	0.841 – 0.876 μm	NIR
4	10.5 - 11.3 μm	TIR	31	10.78 - 11.28 μm	TIR
5	11.5 - 12.5 μm	TIR	32	11.77 - 12.27 μm	TIR

Table 2. The Mean Solar Radiation

Mean Solar Radiation per Month for Cloudless Skies											
JAN	FEB	MAR	APR	MAY	JUN	JUL	AUG	SEP	OCT	NOV	DEC

Latitude	(MJ $m^{-2}d^{-1}$)											
30N	17.46	21.65	25.96	29.85	32.11	33.20	32.66	30.44	26.67	22.48	18.30	16.04
25N	19.68	23.45	27.21	30.14	32.11	32.66	32.24	30.44	27.63	24.28	20.39	18.30
20N	21.65	25.00	28.18	30.14	31.40	31.82	31.53	30.14	28.47	25.83	22.48	20.52
15N	23.57	26.50	29.01	29.85	30.56	30.69	30.56	29.60	29.18	26.92	24.28	22.48

Table 3. The verification of PET calculation from AVHRR and MODIS

	AVHRR		MODIS	
	ME(mm/day)	RMSE	ME(mm/day)	RMSE
Jihyuehtan	1.840	0.931	0.55	0.24
Taipei	1.708	0.904	1.23	0.57
Tainan	1.522	0.684	--	--
Yushan	1.917	0.577	1.07	0.53
Chutzehu	2.658	2.374	1.45	1.90
Alishan	1.901	1.638	1.11	1.00
Hengchun	1.214	0.430	0.80	0.25
Kaohsiung	1.245	0.714	0.75	0.30
Keelung	1.594	0.881	0.83	0.39
Wuchi	1.590	1.108	1.19	0.59
Hsinchu	1.503	1.007	--	--
Chiayi	1.734	0.849	1.25	0.42
Anpu	2.457	2.123	1.03	0.50
Average	1.64	1.11	1.49	1.09

Table 4. The error of meteorological characteristics and sensitivity correction

	RE(%)	RE(%) with sensitivity correction
T	13.2	7.4
VP_{def}	18.5	8.6
R_n	11.0	10.3
u	52.9	9.3

Table 5. The influences of meteorological characteristics

	ME(mm/day)	RE(%)
T	0.25	6.69
VP_{def}	0.28	8.08
R_n	0.35	10.17
u	0.30	8.33

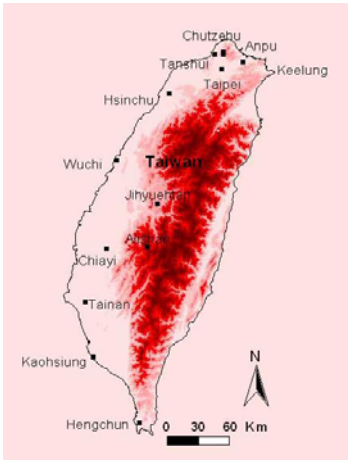

Fig. 1. The main meteorological stations in western Taiwan

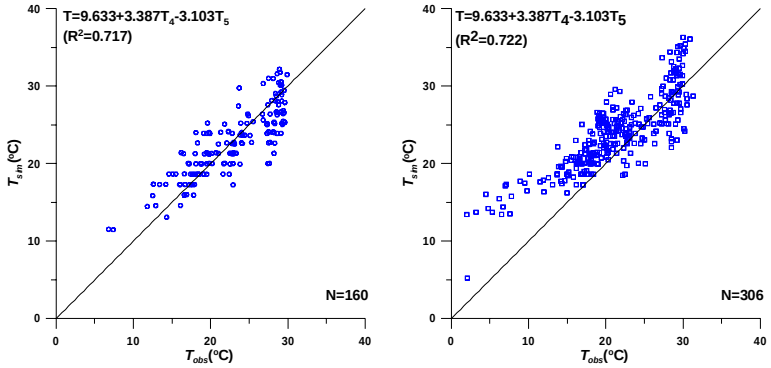

(a) The simulation result (b) The verification result

Fig. 2 The temperature simulation and validation result from AVHRR

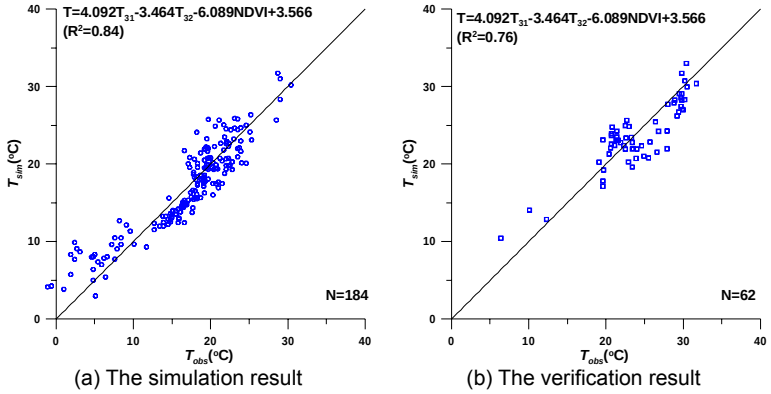

(a) The simulation result (b) The verification result

Fig. 3 The temperature simulation and validation result from MODIS

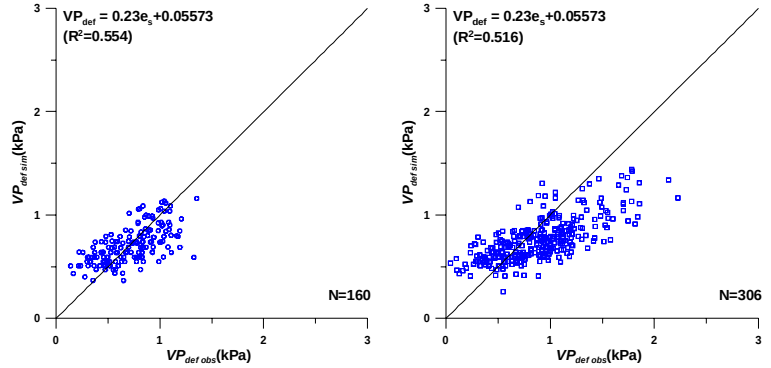

(a) The simulation result (b) The verification result

Fig. 4 The relationship of simulated and observed vapor pressure deficit from AVHRR

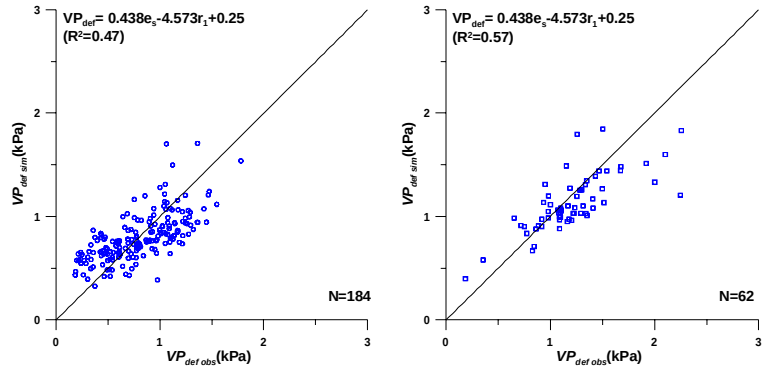

(a) The simulation result (b) The verification result

Fig. 5 The relationship of simulated and observed vapor pressure deficit from MODIS

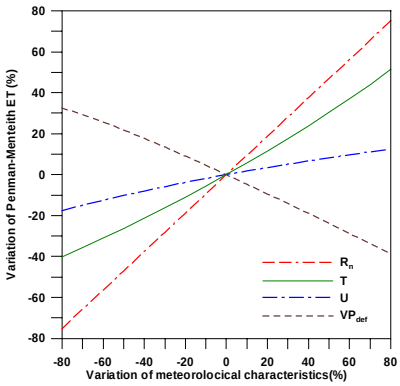

Fig. 6 The sensitivity analysis of meteorological characteristics

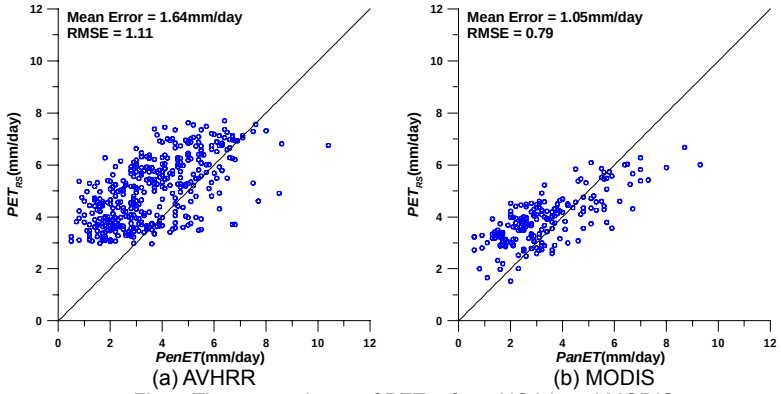

(a) AVHRR (b) MODIS

Fig. 7 The comparisons of PET_{RS} from NOAA and MODIS

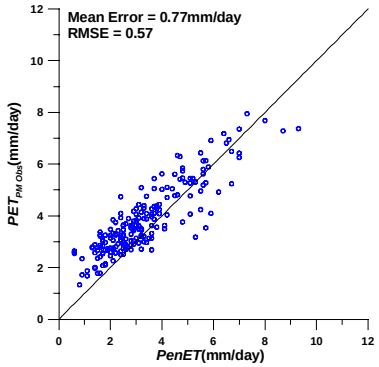

Fig. 8 The comparison of PenET and $PET_{PM\ Obs}$

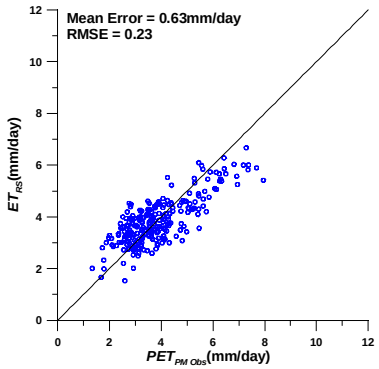

Fig. 9 The comparison of $PET_{PM\ Obs}$ and PET_{RS}